archives
of thermodynamics
Vol. **44**(2023), No. 2, 115–138
DOI: 10.24425/ather.2023.146561

Numerical study of MHD Williamson-nano fluid flow past a vertical cone in the presence of suction/injection and convective boundary conditions

MANTHRI SATHYANARAYANA[a]
TAMTAM RAMAKRISHNA GOUD[b*]

[a] Osmania University, Department of Mathematics, University College of Science, Hyderabad – 500007, Telangana Sate, India

[b] Osmania University, Department of Mathematics, University College of Science, Saifabad, Hyderabad – 500004, Telangana Sate, India

Abstract The primary objective is to perform a numerical synthesis of a Williamson fluid that has nanoparticles added to it and is directed toward a vertical cone in a uniform transverse magnetic field, under heat and mass transport, suction and injection, and convective boundary conditions. For this particular fluid flow, by utilising similarity transformations, the partial differential equations are transformed into ordinary differential equations. Calculating these kinds of equations with their suitable bounds requires the Runge–Kutta technique in combining a shooting strategy. The functions of a vast number of parameters are graphically represented and assessed on flow field profiles. The results show the local skin friction, local Nusselt number, and local Sherwood number and the changing values of the flow constraints. Finally, the results are compared to those from the previously published works and found to be in good agreement.

Keywords: Williamson fluid; Nanofluid; Vertical cone; Suction/Injection; Convective boundary condition

*Corresponding Author. Email: manthrisathyam926@gmail.com

www.czasopisma.pan.pl PAN POLSKA AKADEMIA NAUK www.journals.pan.pl

Nomenclature

a	–	constant
B_o	–	uniform magnetic field, T
Bi	–	Biot number
C	–	fluid nanoparticle volume concentration, mol/m^3
C_w	–	dimensional nanoparticle concentration at the stretching surface
C_∞	–	dimensional ambient volume fraction
C_f	–	skin-friction coefficient, $1/s$
D_B	–	coefficient of Brownian diffusion, m^2/s
D_T	–	coefficient of thermophoresis diffusion, m^2/s
f	–	dimensionless stream function
f'	–	fluid velocity, m/s
Gc	–	Grashof number for mass transfer
Gr	–	Grashof number for heat transfer
g	–	gravitational acceleration, m/s^2
h_1	–	heat transfer coefficient
J_w	–	mass flux coefficient
k^*	–	thermal conductivity of the fluid
L	–	characteristic length, m
M	–	magnetic field parameter
Nb	–	Brownian motion parameter
Nt	–	thermophoresis parameter
Nu	–	Nusselt number
Pr	–	Prandtl number
q_w	–	heat flux coefficient
r	–	radius of the cone, m
r_1	–	wall thermal factor
r_2	–	nanofluid concentration parameter
T	–	fluid temperature, K
T_w	–	surface temperature, K
T_∞	–	temperature of the fluid far from the stretching sheet, K
S	–	suction/injection parameter
Sc	–	Schmidt number
Sh	–	Sherwood number
$u,\ v$	–	x and y directions of velocity components, m/s
$u_w(x)$	–	stretching velocity of the fluid, m/s
v_w	–	suction/injection velocity, m/s
We	–	Williamson fluid parameter
$x,\ y$	–	Cartesian coordinates calculated along the stretching sheet, m

Greek symbols

α	–	half angle of the cone
α^*	–	thermal diffusivity, m^2/s
β_C	–	coefficient of concentration expansion
β_T	–	coefficient of thermal expansion
Γ	–	shear stress, 1/s
η	–	dimensionless similarity variable

www.czasopisma.pan.pl PAN POLSKA AKADEMIA NAUK www.journals.pan.pl

θ – non-dimensional temperature
κ – thermal conductivity of the fluid, W/(mK)
μ – dynamic viscosity of the fluid, Pa s
ν – kinematic viscosity, m^2/s
ρ – density, kg/m^3
σ – Stefan–Boltzmann constant, W/m^2K^4
τ – Ratio of nano particles heat capacity to fluid heat capacity
τ_B – wall shear stress, Nm^{-2}
ϕ – non-dimensional nanoparticle concentration

Subscripts

f – fluid
ρ – nanoparticles
w – condition on the sheet,
∞ – ambient conditions

Superscripts

$(\cdot)'$ – differentiation with respect to η

1 Introduction

Nowadays, non-Newtonian fluids have garnered a lot of attention from hydrodynamics specialists all over the world. This interest may be attributable to the significant scientific advancements that have been made in the applications of this field. In terms of viscosity and the rate of shear stress, the Williamson fluid is remarkably similar to polymeric solutions. Because of this, the Williamson fluid is considered. According to the Williamson fluid model, as the shear rate increased, the viscosity would fall [1]. These flows are often used in a wide variety of industrial applications, including the extrusion of polymer sheets from a die, the production of the boundary layer in processes that include the condensation of liquid films, and the emulsion coating of photographic films. Severa; reseachers examined the Williamson model and, as a consequence of covering a variety of flow patterns, presented a number of different tests, covering a wide range of topics. Aldabesh *et al.* [2] investigated the effects of gyrotactic bacteria on the unsteady flow of Williamson nanofluid using a revolving cylinder. The heat radiation and chemical reaction were examined by Krishnamurthy *et al.* [3] using porous media as the delivery medium. Amer [4] examined the results of numerical simulations of heat flow that made use of Williamson nanofluid MHD and thermal radiation. Loganathan and Rajan [5] investigated Joule

www.czasopisma.pan.pl PAN POLSKA AKADEMIA NAUK www.journals.pan.pl

heating and Williamson nanofluid flow with negligible nanoparticle mass floodway. Dawar *et al.* [6] conducted research to determine which analysis was the most accurate for three-dimensional flow across a stretched surface in convective conditions. Yahya *et al.* [7] studied heat flux on Williamson sutter through the use of nanofluid transportation generated by a stretched surface. This was done in order to better understand how these two heat fluxes interact with Williamson sutter. Sreedevi and Reddy [8] looked at the spinning cylinder with the Cattaneo-Christov heat flux and the gyrotactic microbe. Shafiq and Sindhu's presentation [9] described a Williamson flow that lacked compressibility and was unstable. A unique notion for entropy amplification and activation energy in the transient axis-symmetric flow of Williamson nanofluid was suggested by Azam *et al.* [10]. Ahmed *et al.* [11] investigated the heat transfer mechanism in a Williamson-type fluid in a magnetohydrodynamic (MHD) mixed convection flow over an exponentially stretched porous curved surface. The transfer of heat and mass in Williamson fluid was studied by Nazir *et al.* [12] using generalised non-Fourier models. Kumaran et al. [13] directed research on the impacts of gooey dispersal and intensity moves in a radiative MHD Williamson liquid stream over the top paraboloid of upheaval. At the point when the liquid stream was influenced by the presence of a temperature-subordinate intensity source, Raju *et al.* [14] assessed the Williamson and Casson liquid streams through an extended sheet while thinking about both intensity and mass exchange. It has been accounted for by Bhatti *et al.* [15] that the MHD Williamson nanofluid stream was influenced by gyrotactic microorganisms as it went through spinning round plates. Shateyi *et al.* [16] conducted a thorough investigation into the behaviour of an incompressible conductive Williamson-nanofluid over an extending penetrable sheet. It was conjectured by Nadeem *et al.* [17] that the Williamson liquid stream would happen across an extended sheet.

Nano-fluids are a whole new category of fluids that were invented by Choi [18]. Researchers from all around the world who specialise in studying fluids have shown a great deal of interest in this particular kind of fluid. It is an essential component in a wide variety of today's technological applications that make people's lives easier and more enjoyable. On the other hand, nanofluids have applications in a diverse variety of industries, including the satellite industry. Nanofluids are also vital in the field of medicine. For example, the use of gold nanoparticles in the treatment of cancerous tumours and the assembly of minuscule bombs that are utilised to wipe out destructive tumours are both examples of how nanofluids are employed

www.czasopisma.pan.pl PAN POLSKA AKADEMIA NAUK www.journals.pan.pl

in these fields. Suresh and colleagues [19] produced a hybrid nanofluid by adding nanoparticles to the basic fluids. They claim that this nanofluid surpasses traditional nanofluids in terms of its heat transfer rate. In their study [20], Nadeem and Abbas looked at the behaviour of a micropolar hybrid nanofluid as it moved around a circular cylinder. In addition to this, they emphasised the sliding effects by using a numerical technique. The authors of the study, Devi and Devi [21], conducted their investigation of the hybrid nanofluid at a stretched surface using numerical simulations. Khan *et al.* [22] studied the unsteady flow over a stretched sheet by using a chemical reaction in their research. Lu *et al.* [23] investigated the flow of hybrid nanofluids through a curved surface as part of their research. Khan *et al.* [24] placed a strong focus on the significance of activation energy in relation to chemical processes. Khan *et al.* [25] employed computer simulations to research the flow of a nonlinear radiative fluid that was coupled with a chemical process. Khan *et al.* [26] researched and represented the conditions directing the MHD radiative nanofluid stream with heat age and substance responses toward a wedge. They found that these equations guide the flow of nanofluids under MHD conditions. Motsumi and Makinde [27] explored heat radiation and viscous dissemination in nanofluids as they went through a formerly level subsurface. Rana *et al.* [28] determined how much entropy is created by a nanofluid slip stream when exposed to the impact of the Stefan blowing impact by utilising a changed form of the Buongiorno model. Qing Song and colleagues [29] investigated the flow of a topsy-turvy turning circle. Alsabery *et al.* [30] took a gander at the impact that half-breed nanofluid has on the properties of a blended convection stream in a cover-driven pit. Turkyilmazoglu *et al.* [31] discussed the intensity exchange of nanofluid streams as they passed through an infinitely high-level plate. They did this while considering the effects of radiation caused by two different types of warm boundary conditions. In order to solve the problem of spinning Maxwell liquid in a three-dimensional nano-fluid while it was being hit by an ever-expanding surface, Hayat *et al.* [32] used the homotopy research approach. Sheikholeslami and Shehzad [33] looked into the heat transport of a non-equilibrium nanofluid in the presence of an attractive field and a permeable medium. Their research was published in the journal Nano Letters. The bio-convection of nanofluid through a porous surface that extends vertically was shown by Sarkar *et al.* [34]. Rao *et al.* [37] studied three-dimensional flow of inclined magneto Carreau nanofluid with chemical reactions. Sathyanarayana *et al.* [38] studied the characteristics of MHD nanofluid flow towards a vertical cone under convective cross-diffusion

www.czasopisma.pan.pl PAN POLSKA AKADEMIA NAUK www.journals.pan.pl

effects. Archana *et al.* [39] focused on the bidirectionally stretched flow of a Jeffrey liquid with nanoparticles.

This work is persuaded by the past exploration works, and its goal is to research the progression of a two-layered magnetohydrodynamics (MHD) Williamson-nanofluid across an upward cone with heat transfer, mass transfer, pull/infusion, and convective boundary conditions. The review will likely figure out additional details about these parts of the stream. The halfway differential conditions (partial differential equations, PDEs) are controlled by the fundamental Navier-Stokes equation and the Williamson liquid model, and fitting similitude changes are used to transform them into customary differential conditions (ordinary differential equations, ODEs). The conventional differential equations that result are then mathematically addressed using the Runge–Kutta method. The effects of a variety of various physical parameters on the temperature, velocity, and concentration profiles are shown using graphs and tables.

2 Flow governing equations

This research investigates the heat and mass transfer in a continuous flow of Williamson-nanofluid that is viscous and incompressible around a vertical cone when suction/injection and convective boundary conditions are present. The flow is described as being around the cone. The physical coordinates and the geometry of the issue are shown in Fig. 1. The following presumptions have been made with regard to this project:

- The limit calculations are forced by circumstances.
- Brownian movement impacts are likewise thought of.
- The stretching velocity of the surface is taken as $u_w = \dfrac{x\nu}{L^2}$ whereas the suction/injection velocity is denoted as v_w.
- The surface temperature is taken as $T_w = T_\infty + ax^{r_1}$ where $a$is a constant and r_1 is the wall thermal factor.
- The concentration near the surface is expressed as $C_w = C_\infty + ax^{r_2}$ where a is a constant and r_2 is the nanofluid concentration parameter.
- The half place of the cone is given by α, with sweep r of the cone.

www.czasopisma.pan.pl PAN POLSKA AKADEMIA NAUK www.journals.pan.pl

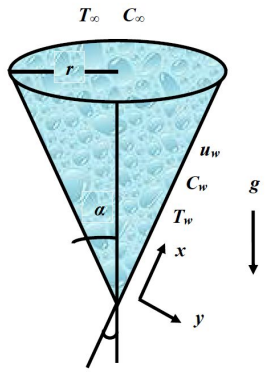

Figure 1: Geometry representation of the fluid flow.

- In light of the above presumptions, the governing equations for consistent, two-layered, electrically directing, incompressible, Williamson-nanoliquid stream are:

Continuity equation:

$$\frac{\partial u}{\partial x}+\frac{\partial v}{\partial y}=0. \tag{1}$$

Momentum equation:

$$u\frac{\partial u}{\partial x}+v\frac{\partial u}{\partial y}=\nu\frac{\partial^2 u}{\partial y^2}+\sqrt{2}\nu\Gamma\frac{\partial u}{\partial y}\frac{\partial^2 u}{\partial y^2}-\left(\frac{\sigma B_o^2}{\rho_f}\right)u + g\left[\left(1-C_\infty\right)\rho\beta_T\left(T-T_\infty\right)-\beta_C\left(\rho_p-\rho_f\right)\left(C-C_\infty\right)\right]\cos\alpha. \tag{2}$$

Equation of thermal energy:

$$u\frac{\partial T}{\partial x}+v\frac{\partial T}{\partial y}=\alpha^*\frac{\partial^2 T}{\partial y^2}+\tau_B\left[D_B\frac{\partial C}{\partial y}\frac{\partial T}{\partial y}+\frac{D_T}{T_\infty}\left(\frac{\partial T}{\partial y}\right)^2\right]. \tag{3}$$

Equation of species nanoparticle volume concentration:

$$u\frac{\partial C}{\partial x}+v\frac{\partial C}{\partial y}=D_B\frac{\partial^2 C}{\partial y^2}+\frac{D_T}{T_\infty}\frac{\partial^2 T}{\partial y^2}. \tag{4}$$

The boundary conditions for this flow are:

$$\left.\begin{aligned} u=u_w,\quad v=-v_w(x),\quad -k^*\left(\frac{\partial T}{\partial y}\right)=h_1\left(T_w-T\right),\\ D_B\left(\frac{\partial C}{\partial y}\right)+\frac{D_T}{T_\infty}\left(\frac{\partial T}{\partial y}\right)=0\quad\text{at}\quad y=0,\\ u\to 0,\quad T\to T_\infty,\quad C\to C_\infty\quad\text{as}\quad y\to\infty. \end{aligned}\right\} \tag{5}$$

www.czasopisma.pan.pl PAN POLSKA AKADEMIA NAUK www.journals.pan.pl

The following similarity transformations are introduced

$$u = \frac{x\nu}{L^2} f'(\eta), \quad v = -\frac{\nu}{L} f(\eta), \quad \theta = \frac{T - T_\infty}{T_w - T_\infty}, \quad \phi = \frac{C - C_\infty}{C_w - C_\infty}, \quad \eta = \frac{y}{L}. \tag{6}$$

Making help of Eq. (6), the continuity equation is identically fulfilled and Eqs. (2)–(4) get the subsequent forms:

$$f''' + ff'' + \mathrm{We} f''' f'' - \mathrm{We} f' - f'^2 + \mathrm{Gr}\theta\cos\alpha + \mathrm{Gc}\phi\cos\alpha = 0, \tag{7}$$

$$\theta'' + \mathrm{Pr}\, f\theta' - \mathrm{Pr}\, r_1 f'\theta + \mathrm{Pr}\,\mathrm{Nb}\theta'\phi' + \mathrm{Pr}\,\mathrm{Nt}(\theta')^2 = 0, \tag{8}$$

$$\mathrm{Nb}\phi'' + \mathrm{Sc} f\phi' - \mathrm{Sc} r_2 f'\phi + \mathrm{Sc}\,\mathrm{Nt}\theta'' = 0, \tag{9}$$

and the corresponding boundary conditions (5) become:

$$\begin{gathered} f(0) = \mathrm{S}, \quad f'(0) = 1, \quad \theta'(0) = \mathrm{Bi}\,[\theta(0) - 1], \quad \mathrm{Nb}\phi'(0) + \mathrm{Nt}\theta'(0) = 1, \\ f'(\infty) \to 0, \quad \theta(\infty) \to 0, \quad \phi(\infty) \to 0, \end{gathered} \tag{10}$$

where the involved physical parameters are defined as:

$$\begin{aligned} &\mathrm{We} = \frac{2\sigma B_o^2 L}{\rho_f}, \quad \mathrm{Pr} = \frac{\alpha}{\mu C_p}, \quad \mathrm{Nb} = \frac{\tau D_B\,(C_w - C_\infty)\,h}{\nu}, \\ &\mathrm{Nt} = \frac{\tau D_T\,(T_w - T_\infty)}{\nu T_\infty}, \quad \mathrm{We} = \frac{\sqrt{2}\Gamma}{L} u_w, \\ &\mathrm{Bi} = \frac{Lh_1}{k^*}, \quad \mathrm{Gr} = \frac{gL^2\beta_T\,(T_w - T_\infty)}{\nu u_w}, \\ &\mathrm{Gc} = \frac{gL^2\beta_C\,(C_w - C_\infty)}{\nu u_w}, \quad \mathrm{S} = \frac{v_w L}{\nu}. \end{aligned} \tag{11}$$

Quantities of actual interest, the actual boundaries of the skin-friction coefficient, the nearby Nusselt number and neighbourhood Sherwood number are introduced as follows:

$$\begin{aligned} C_f &= \frac{\tau_w}{\rho u_w^2} = \frac{1}{\rho\left(\dfrac{x\nu}{L^2}\right)} \mu \left[\frac{\partial u}{\partial y} + \frac{\Gamma}{\sqrt{2}}\left(\frac{\partial u}{\partial y}\right)^2\right]_{y=0} \\ &\Rightarrow C_f = f''(0) + \frac{\mathrm{We}}{2}\left[f''(0)\right]^2, \end{aligned} \tag{12}$$

$$\mathrm{Nu} = \frac{xq_w}{\kappa\,(T_w - T_\infty)} = \frac{\left[-x\dfrac{\partial T}{\partial y}\right]_{y=0}}{\kappa\,(T_w - T_\infty)} = -\theta'(0), \tag{13}$$

www.czasopisma.pan.pl PAN POLSKA AKADEMIA NAUK www.journals.pan.pl

$$\mathrm{Sh} = \frac{xJ_w}{D_B\,(C_w - C_\infty)} = \frac{\left[-x\dfrac{\partial C}{\partial y}\right]_{y=0}}{D_B\,(C_w - C_\infty)} = -\phi'(0). \tag{14}$$

3 Method of solution

The Runge–Kutta method, along with the shooting approach, can solve non-linear governing equations in terms of partial derivatives. The procedure for this method is shown in Fig. 2. Other numerical approaches provide less precise results than this method. Using similarity transformations, the controlling halfway differential conditions are transformed into common differential conditions. Utilizing extra factors, non-straight conditions are changed over completely to direct conditions. For the conversion of higher

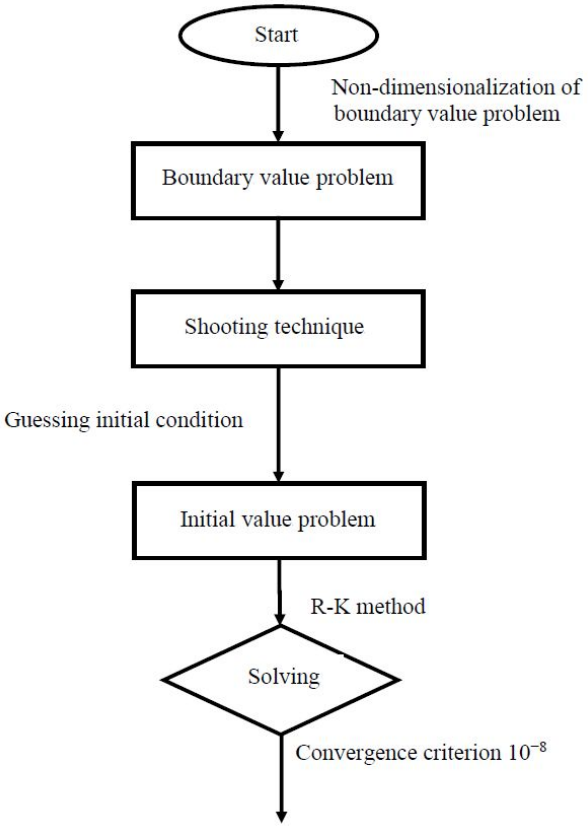

Figure 2: Flow diagram of the numerical procedure.

www.czasopisma.pan.pl PAN POLSKA AKADEMIA NAUK www.journals.pan.pl

order to linear differential equations, the following additional variables are introduced:

$$f_1 = f, \quad f_2 = f', \quad f_3 = f'', \quad f_4 = \theta, \quad f_5 = \theta', \quad f_6 = \phi, \quad f_7 = \phi'. \tag{15}$$

Equations (7)–(9) are transformed to the following first order ODEs:

$$\begin{aligned} f_3 &= f_2', \\ f_3' &= -f_1 f_3 - \mathrm{We} f_3' f_3 + \mathrm{We} f_2 + f_2^2 - \mathrm{Gr} f_4 \cos\alpha - \mathrm{Gc} f_6 \cos\alpha, \\ f_5' &= -\mathrm{Pr}\, f_1 f_5 + \mathrm{Pr}\, r_1 f_2 f_4 - \mathrm{Pr}\,\mathrm{Nb} f_5 f_7 - \mathrm{Pr}\,\mathrm{Nt} f_5^2, \\ f_7' &= -\frac{1}{\mathrm{Nb}} \left(-\mathrm{Sc} f_1 f_7 + \mathrm{Sc} r_2 f_2 f_6 - \mathrm{Sc}\,\mathrm{Nt} f_5'\right). \end{aligned} \tag{16}$$

Using Eq. (16), the corresponding boundary conditions (10) are:

$$\begin{aligned} &f_1(0) = \mathrm{S}, \quad f_2(0) = 1, \quad f_5(0) = \mathrm{Bi}\left[f_4(0) - 1\right], \\ &\mathrm{Nb} f_7(0) + \mathrm{Nt} f_5(0) = 1, \\ &f_2(\infty) \to 0, \quad f_4(\infty) \to 0, \quad f_6(\infty) \to 0. \end{aligned} \tag{17}$$

To demonstrate the physical relevance of non-dimensional parameters, the approximate solutions are numerically derived, resulting in a graphical representation using MATLAB bvp4c programming. The iterative approach is repeated until we achieve data that are accurate to a precision of 10^{-6}.

4 Program code validation

For the accuracy and approval of the ongoing model, the current discoveries connected with the skin-friction coefficient and Nusselt number outcomes are contrasted with those of Vajravelu and Nayfeh [35] and Chamkha [36] as shown in Tables 1 and 2.

Table 1: Evaluation of the present skin-friction number results with the previously published skin-friction number results for various r_1.

r_1	Vajravelu and Nayfeh [35]	Chamkha [36]	Present Nusselt number results
–2.1	0.155592	0.155592	0.155488203126587
2.0	0.156001	0.155995	0.155862001723045

Table 2: Evaluation of the present Nusselt number results with the previously published Nusselt number results for various r_1.

r_1	Vajravelu and Nayfeh [35]	Chamkha [36]	Present Nusselt number results
–2.1	2.237475	2.238739	2.228503154257842
2.0	2.232780	2.234070	2.227400532610918

5 Results and discussion

After converting the system of partial differential equations used to study the flow of fluid into a system of ordinary differential equations, it has a set of important parameters that we list in the following order: We, M, Gr and Gc which are the Williamson liquid parameter, magnetic field, thermal Grashof number and solutal Grashof number, while S, Pr, Bi and r_1 represent the suction/injection, Prandtl number, Biot number and thermal wall concentration parameters, respectively; also, r_2, Nb, Nt and Sc are the solutal wall concentration, Brownian motion, thermophoresis and Schmidt number, respectively. The effect of all the previous physical parameters on the velocity, temperature, and concentration distributions has been studied by making graphical figures that clarify this and by showing the physical meanings of each parameter and its importance in this study.

Figure 3 shows the effects of the Williamson fluid parameter on the velocity profile. By increasing the Williamson fluid parameter, there is an increase in the value of velocity. This behaviour is well understood by the physics of the Williamson fluid parameter.

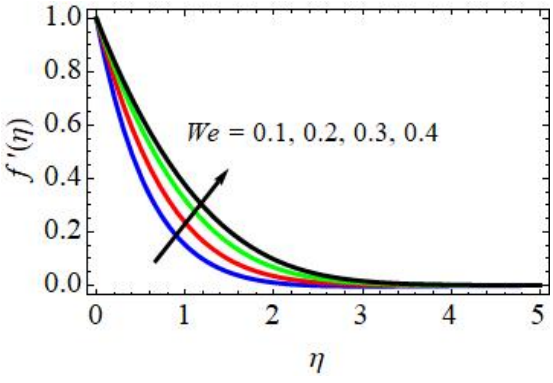

Figure 3: We impact on velocity.

www.czasopisma.pan.pl PAN POLSKA AKADEMIA NAUK www.journals.pan.pl

Figures 4 and 5 show the impact of the magnetic field parameter (M) on the flow velocity and temperature, respectively. The fluid velocity was found to decrease and the temperature was found to increase as the magnetic field increased between 0.5, 0.8, 1.0, and 1.2. This is on the grounds that the attractive field gives what is known as a Lorentz force, which is a decelerating body force that acts in the opposite direction to the actual magnetic field. On account of this body force, the progression of the boundary layer as well as the thickness of the energy boundary layer are both decreased. Likewise, it produces heat due to the Lorentz force, which is a fragmentary resistive power that neutralises the velocity of the liquid. In view of this property, the warm boundary layer will be more prominent in thickness when the magnetic field is stronger.

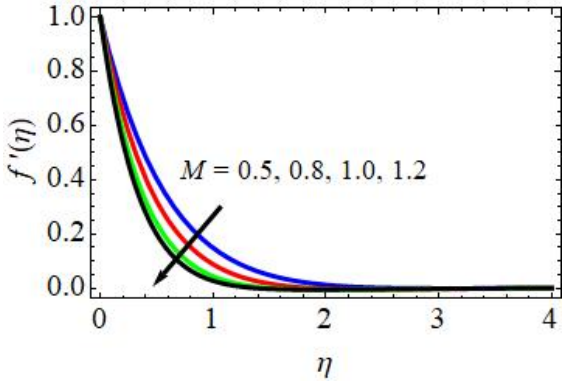

Figure 4: M impact on velocity.

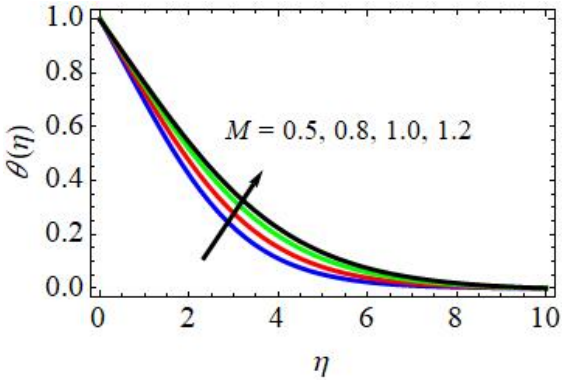

Figure 5: M influence on temperature.

www.czasopisma.pan.pl PAN POLSKA AKADEMIA NAUK www.journals.pan.pl

Figure 6 indicates the effect of thermal Grashof number (Gr) on the velocity distribution for a cone. The increased Grashof number enhances the velocity distribution for cones. The increased thermal Grashof number reduces the viscosity of the nanofluid, which decreases the boundary layer thickness. Thus, the reduced viscosity of the nanofluid flow increases the velocity distribution. Figure 7 shows the impact of the solutal Grashof number (Gc) on the velocity distribution. A similar response of the solutal Grashof number to the thermal Grashof number is depicted here. It is noteworthy that the solutal Grashof number has a greater effect for a wedge as compared to a cone. In addition, when Gr = 0 and Gc = 0, the phenomenon has no thermal or solutal buoyancy forces.

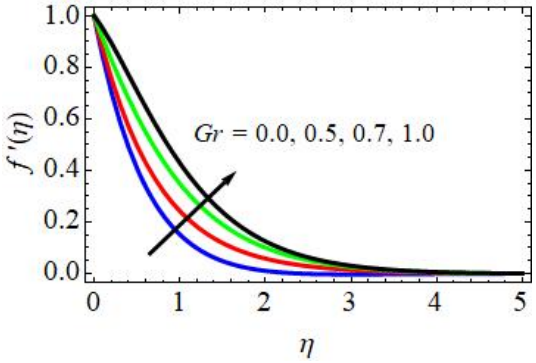

Figure 6: Gr influence on velocity.

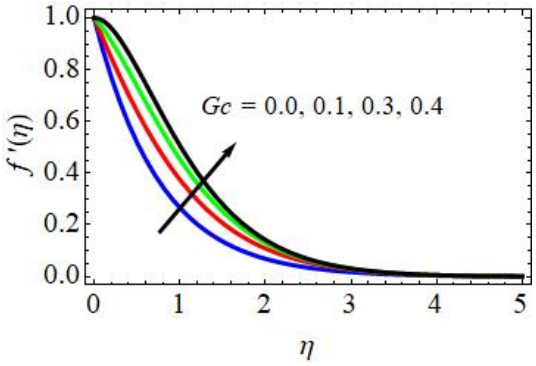

Figure 7: Gc impact on velocity.

Figure 8 illustrate the effect of suction/injection parameter (S) on velocity profiles. The suction/injection parameter controls fluid flow. It is easy to

www.czasopisma.pan.pl PAN POLSKA AKADEMIA NAUK www.journals.pan.pl

discern that for greater values of S the velocity profile tends to decrease. For $S < 0$ (injection), the fluid nearest the boundary boosts which increases the flow velocity and the collision between the molecules, which in turn causes an increase in the internal kinetic energy. On the other hand, for $S > 0$ (suction), the fluid near the boundary is sucked, which creates porosity near the boundary, which in turn reduces the velocity profile. Figure 9 shows the impact of the suction/injection parameter (S) on the dimensionless velocity profiles. The curves in Fig. 9 show that the parameter S affects the thickness of the boundary layer. With the rising S, the flow appears to decelerate dramatically. The border layer adheres more tightly to the wall because of suction/injection. As a result, momentum is lost, resulting in a decrease in velocity. As a result of suction/injection, the thickness of the energy boundary layer is decreased.

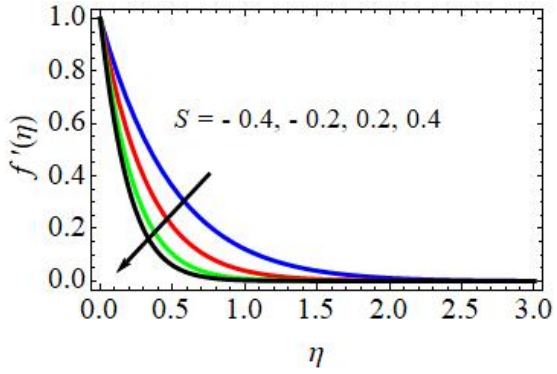

Figure 8: S impact on velocity.

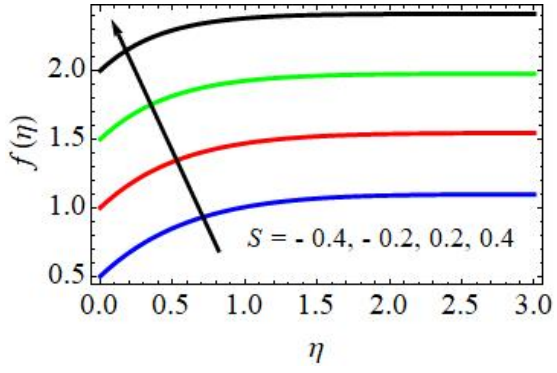

Figure 9: S impact on velocity.

www.czasopisma.pan.pl PAN POLSKA AKADEMIA NAUK www.journals.pan.pl

An illustration of the impact of the Prandtl number (Pr) on temperature profiles is presented in Fig. 10 Increased Prandtl numbers over a certain threshold indicate that the temperature is decreased. When the thermal diffusivity and Prandtl number are inverted, a cooling effect is seen. Figure 11 delineates that the warm Biot number has a direct connection with temperature distributions. Figure 11 depicts the upsides of warm increments. The thermal Biot number increase (Bi $>$ 0) means that the heat transfer rate increases, which causes an increase in the temperature profile.

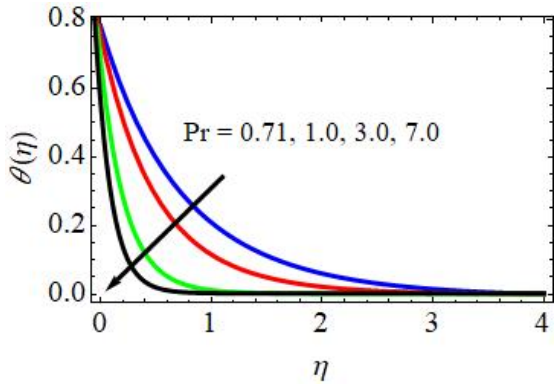

Figure 10: Pr impact on temperature.

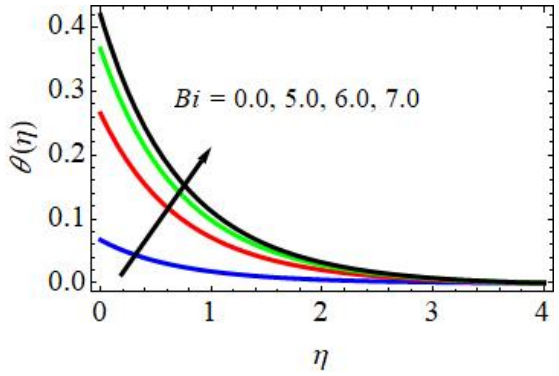

Figure 11: Bi impact on temperature.

Figures 12 and 13 show the impact of the thermal wall factor (r_1) and nanofluid concentration parameter (r_2) on non-dimensional temperature and nanoparticle concentration profiles for a cone. Both the thermal and concentration distributions are reducing functions of wall concentration.

www.czasopisma.pan.pl PAN POLSKA AKADEMIA NAUK www.journals.pan.pl

The boundary layer thickness declines with the greater wall concentration. Thus, the reduction in temperature and concentration of the nanofluid flow is depicted.

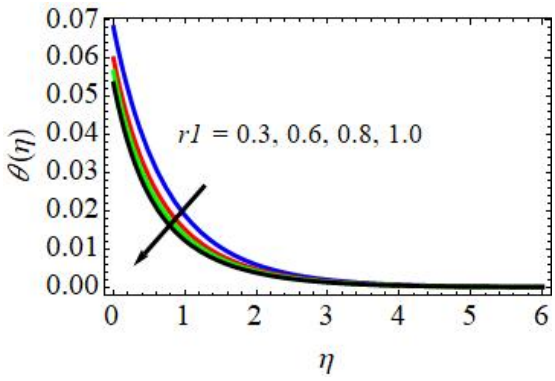

Figure 12: r_1 impact on temperature.

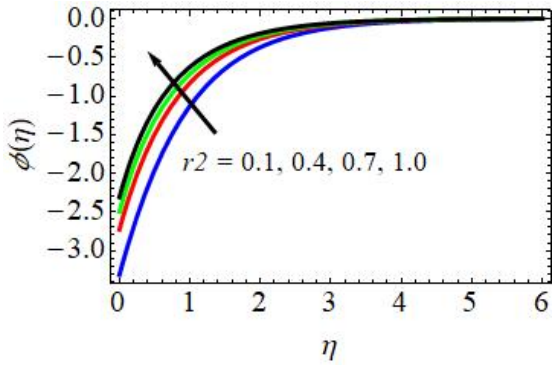

Figure 13: r_2 impact on concentration.

The impact of the Brownian motion parameter (Nb) on temperature and concentration profiles is displayed in Figs. 14 and 15. Figures 14 and 15 show that as the Brownian motion parameter rises, both the temperature and concentration rise.

Figures 16 and 17 uncover the effect of thermophoresis parameter (Nt) on temperature and concentration profiles. Both profiles increase with higher potential gains of Nt. Thermophoresis is the transport force that occurs due to the temperature gradient between layers of the fluid. A higher thermophoresis parameter means that the temperature difference between the

www.czasopisma.pan.pl PAN POLSKA AKADEMIA NAUK www.journals.pan.pl

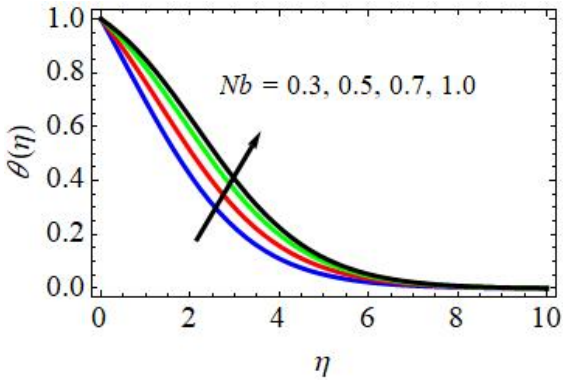

Figure 14: Nb impact on temperature.

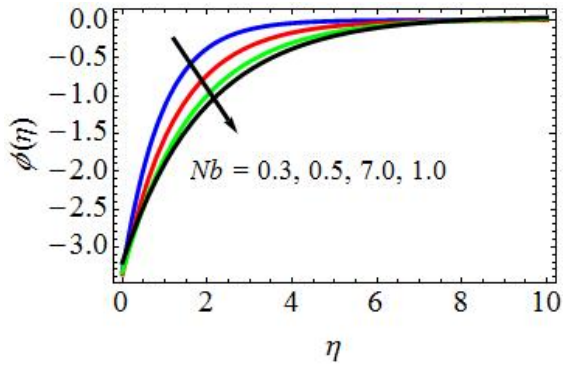

Figure 15: Nb impact on concentration.

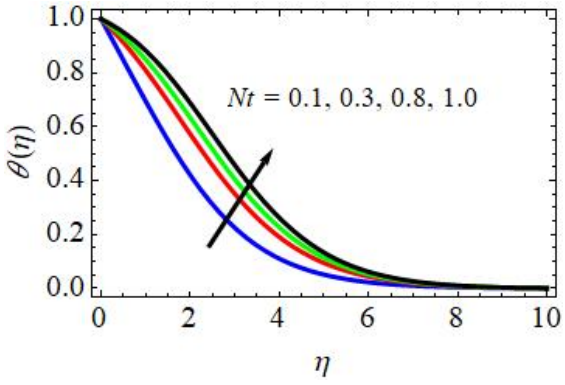

Figure 16: Nt impact on temperature.

www.czasopisma.pan.pl PAN POLSKA AKADEMIA NAUK www.journals.pan.pl

layers increases, so the heat transfer rate also increases. By increasing the nanoparticles, the concentration of the fluid increases. With more nanoparticles and more heat transfer between the layers, as Nt increase s, both the temperature and concentration profiles have increased values.

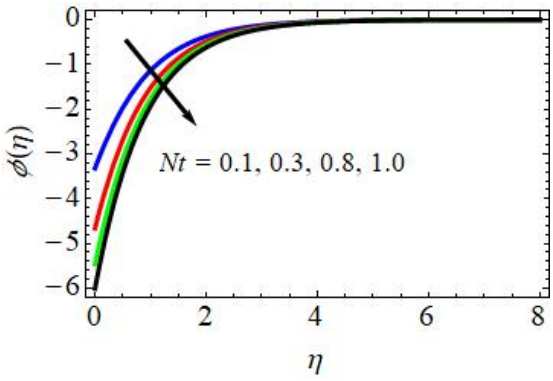

Figure 17: Nt impact on concentration.

Figure 18 depicts the impact of Schmidt number (Sc) on the concentration profile showing that the expanding Sc diminishes the concentration profile since Sc is the proportion of the kinematic viscosity to the molecular diffusion rate.

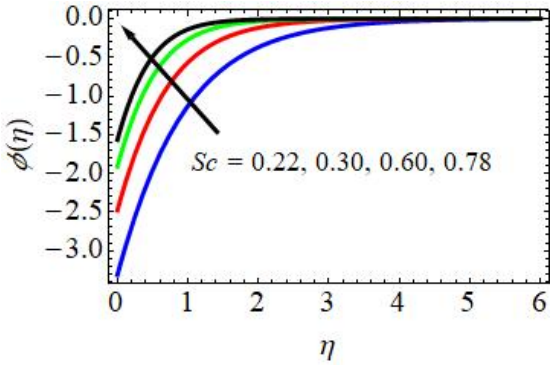

Figure 18: Sc influence on concentration profiles.

Table 3 shows the numerical values of skin-friction coefficient for varying values of the engineering parameters such as We, M, Gr, Gc, Pr, S, Bi, r_1, r_2, Nb, Nt and Sc. From this table, it is observed that the skin-friction coefficient increases with the rising values of Gr, Gc, Bi, Nb, Nt, while it

www.czasopisma.pan.pl PAN POLSKA AKADEMIA NAUK www.journals.pan.pl

decreases with the increasing values of We, M, Pr, S, r_1, r_2 and Sc. The numerical values of heat transfer coefficient in terms of the Nusselt number are displayed in Table 4 for different values of Pr, Bi, r_1, Nb and Nt. The heat transfer coefficient gradually rises with the increasing values of Bi, Nb, Nt while the reverse effect is observed for the increasing values of Pr and r_1. The effects of Sc, r_2, Nb and Nt on the mass transfer coefficient in terms of the Sherwood number coefficient are discussed in Table 5. From this table, it is observed that the mass transfer coefficient increases with

Table 3: Skin-friction coefficient (C_f) for various We, M, Gr, Gc, Pr, S, Bi, r_1, r_2, Nb, Nt and Sc.

We	M	Gr	Gc	Pr	S	Bi	r_1	r_2	Nb	Nt	Sc	C_f
0.1	0.5	0.5	0.1	0.71	–0.4	5.0	0.3	0.1	0.3	0.1	0.22	1.263774585842895
0.2												1.227465743637469
0.3												1.176965909390956
	0.8											1.216574017409364
	1.0											1.185683746349504
		0.7										1.302680743987436
		1.0										1.338609348608739
			0.3									1.316758374183899
			0.4									1.346508346984842
				1.0								1.209852676358384
				3.0								1.165787638708037
					–0.2							1.240567896438927
					0.2							1.227678956041874
					0.4							1.205671346648317
						6.0						1.295704360376410
						7.0						1.318578036473463
							0.6					1.236587634806086
							0.8					1.217693960734634
								0.4				1.230738976903837
								0.7				1.214585489259855
									0.5			1.297692365906361
									0.7			1.327651076736500
										0.3		1.307936705163089
										0.8		1.337651756108073
											0.30	1.227693916334563
											0.60	1.216873680746348

www.czasopisma.pan.pl PAN POLSKA AKADEMIA NAUK www.journals.pan.pl

the increasing values of Nt and decreases with the increasing values of Sc, r_2 and Nb.

Table 4: Nusselt number for various Pr, Bi, r_1, Nb and Nt.

Pr	Bi	r_1	Nb	Nt	Nu
0.71	5.0	0.3	0.3	0.1	0.349569273975659
1.0					0.303476376573034
3.0					0.286597362937563
	6.0				0.365643377877981
	7.0				0.376982396736472
		0.6			0.317537924073740
		0.8			0.297673969724909
			0.5		0.375676872391038
			0.7		0.398576124087621
				0.3	0.382298459127092
				0.8	0.406976301073374

Table 5: The rate of mass transfer coefficient for different values of Sc, r_2, Nb and Nt.

Sc	r_2	Nb	Nt	Sh
0.22	0.1	0.3	0.1	0.410696923637232
0.30				0.366739692394710
0.60				0.347593477650983
	0.4			0.375657034347986
	0.7			0.354768973991028
		0.5		0.372654701576319
		0.7		0.356767895753858
			0.3	0.436560564563508
			0.8	0.453767901612703

6 Conclusions

In this article, the two-layered, viscous, incompressible, electrically directed attractive progression of the Williamson nanofluid towards an upward cone in the presence of heat and mass transfer was considered. On the other hand, the basic governing partial differential equations were converted into a system of ordinary differential equations using similarity transformations and

www.czasopisma.pan.pl PAN POLSKA AKADEMIA NAUK www.journals.pan.pl

the non-dimensional variables under the impacts of the Williamson fluid parameter and magnetic field, Biot number and thermal wall focus, solutal wall fixation, Brownian movement, thermophoresis and Schmidt number on dispersion of velocity, temperature and concentration. The main conclusion drawn from this study are the following:

1. The velocity distribution of the fluid flow is negatively affected by the influence of the magnetic field parameter, the Williamson fluid parameter, and suction or injection, and positively affected by the influence of the thermal Grashof number and the solutal Grashof number.

2. The enhancement in the values of Biot number, thermophoresis number, and Brownian motion resulted in an enhancement of the temperature of the fluid flow, while the opposite occurs with the increasing values of Prandtl number and thermal wall concentration parameters.

3. It was found that the distribution of the concentration of nanoparticles decreased under the influence of Schmidt number, Brownian motion coefficient and solutal wall concentration parameter, while the reverse effect was observed in the presence of the thermophoresis coefficient.

Received 20 November 2022

References

[1] Williamson R.V.: *The flow of pseudoplastic materials.* Ind. Eng. Chem. **21**(1929), 11, 1108–1111.

[2] Aldabesh A., Khan S.U., Habib D., Waqas H., Tlili I., Khan M.I., Khan W.A.: *Unsteady transient slip flow of Williamson nanofluid containing gyrotactic microorganism and activation energy.* Alexandria Eng. J. **59**(2020), 6, 4315–4328.

[3] Krishnamurthy M.R., Prasannakumara B.C., Gireesha B.J., Gorla R.S.R.: *Effect of chemical reaction on MHD boundary layer flow and melting heat transfer of Williamson nanofluid in porous medium.* Eng. Sci. Technol. **19**(2016), 1, 53–61.

[4] M. Amer Q.: *Numerical simulation of heat transfer flow subject to MHD of Williamson nanofluid with thermal radiation.* Symmetry. **13**(2020), 1, 1–10.

[5] Loganathan K., Rajan S.: *An entropy approach of Williamson nanofluid flow with joule heating and zero nanoparticle mass flux.* J. Therm. Anal. Calorim. **141**(2020), 6, 2599–2612.

www.czasopisma.pan.pl PAN POLSKA AKADEMIA NAUK www.journals.pan.pl

[6] Dawar A., Shah Z., Islam S., Khan W., Idrees M.: *An optimal analysis for Darcy-Forchheimer three-dimensional Williamson nanofluid flow over a stretching surface with convective conditions*. Adv. Mech. Eng. **11**(2019), 3, 1687814019833510.

[7] Yahya A.U., Salamat N., Habib D., Ali B., Hussain S., Abdal S.: *Implication of bio-convection and Cattaneo-Christov heat flux on Williamson sutter by nanofluid transportation caused by a stretching surface with convective boundary*. Chinese J. Phys.**73**(2021), 706–718.

[8] Sreedevi P., Reddy P.S.: *Williamson hybrid nanofluid flow over swirling cylinder with Cattaneo-Christov heat flux and gyrotactic microorganism*. Wave Random Complex Med. (2021), 1–28. doi: 10.1080/17455030.2021.1968537.

[9] Shafiq A., Sindhu T.N.: *Statistical study of hydromagnetic boundary layer flow of Williamson fluid regarding a radiative surface*. Results Phys. **7**(2017), 3059–3067.

[10] Azam M., Mabood F., Xu T., Waly M., Tlili I.: *Entropy optimized radiative heat transportation in axisymmetric flow of Williamson nanofluid with activation energy*. Results Phys. **19**(2020), 103576.

[11] Ahmed K., Khan W.A., Akbar T., Rasool G., Alharbi S.O., Khan I.: *Numerical investigation of mixed convective Williamson fluid flow over an exponentially stretching permeable curved surface*. Fluids **6**(2021), 7, 260.

[12] Nazir U., Sadiq M.A., Nawaz M.: *Non-Fourier thermal and mass transport in hybridnano-Williamson fluid under chemical reaction in Forchheimer porous medium*. Int. Commun. Heat Mass Transfer. **127**(2021), 105536.

[13] Kumaran G., Sandeep N., Vijayaragavan R.: *Melting heat transfer in magnetohydrodynamic radiative Williamson fluid flow with non-uniform heat source/sink*. IOP Conf. Ser.: Mater. Sci. Eng. **263**(2017), 6, 062022.

[14] Raju C.S., Sandeep N., Ali M.E., Nuhait A.O.: *Heat and mass transfer in 3-D MHD Williamson-casson fluids flow over a stretching surface with non-uniform heat source/sink*. Therm. Sci. **23**(2019), 1, 281–293.

[15] Bhatti M., Arain M., Zeeshan A., Ellahi R., Doranehgard M.: *Swimming of gyrotactic microorganism in MHD Williamson nanofluid flow between rotating circular plates embedded in porous medium: Application of thermal energy storage*. J. Energ. Stor. **45**(2022), 103511.

[16] Shateyi S., Muzara H.: *On the numerical analysis of unsteady MHD boundary layer flow of Williamson fluid over a stretching sheet and heat and mass transfers*. Computation **8**(2020), 2, 30–55.

[17] Nadeem S., Hussain S.T., Lee C.: *Flow of a Williamson fluid over a stretching sheet*. Braz. J. Chem. Eng. **30**(2013), 3, 619–625.

[18] Choi S.U.S., Eastman J.A.: *Enhancing thermal conductivity of fluids with nanoparticles*. In: Proc. ASME Int. Mechanical Engineering Cong. Expo., San Francisco, 12–17 Nov. 1995, 196525.

[19] Suresh S., Venkitaraj K.P., Selvakumar P., Chandrasekar M.: *Effect of Al_2O_3-Cu/water hybrid nanofluid in heat transfer*. Exp. Thermal Fluid Sci. **38**(2012), 54–60.

[20] Nadeem S., Abbas N.: *On both MHD and slip effect in micropolar hybrid nanofluid past a circular cylinder under stagnation point region*. Can. J. Phys. **97**(2018), 4, 392–399.

www.czasopisma.pan.pl PAN POLSKA AKADEMIA NAUK www.journals.pan.pl

[21] Devi S.S.U.: *Numerical investigation of three-dimensional hybrid Cu-Al2O3/water nanofluid flow over a stretching sheet with effecting Lorentz force subject to Newtonian heating*. Can. J. Phys. **94**(2016), 5, 490–496.

[22] Khan W.A., Alshomrani A.S., Alzahrani A.K., Khan M., Irfan M.: *Impact of autocatalysis chemical reaction on nonlinear radiative heat transfer of unsteady three-dimensional Eyring-Powell magneto-nanofluid flow*. Pramana **91**(2018), 5, 1–9.

[23] Lu D., Ramzan M., Ahmad S., Shafee A., Suleman M.: *Impact of nonlinear thermal radiation and entropy optimization coatings with hybrid nanoliquid flow past a curved stretched surface*. Coatings **8**(2018), 12, 414–430.

[24] Khan W. A., Sultan F., Ali M., Shahzad M., Khan M., Irfan M.: *Consequences of activation energy and binary chemical reaction for 3D flow of cross-nanofluid with radiative heat transfer*. J. Braz. Soc. Mech. Sci. Eng. **41**(2019), 1, 1–13.

[25] Khan W.A., Ali M., Sultan F., Shahzad M., Khan M., Irfan M.: *Numerical interpretation of autocatalysis chemical reaction for nonlinear radiative 3D flow of cross magneto-fluid*. Pramana **92**(2019), 2, 1–16.

[26] Khan M.S., Karim I., Islam M. S., Wahiduzzaman M.: *MHD boundary layer radiative, heat generating and chemical reacting flow past a wedge moving in a nanofluid*. Nano Converg. **1**(2014), 1, 1–13.

[27] Motsumi T.G., Makinde O.D.: *Effects of thermal radiation and viscous dissipation on boundary layer flow of nanofluids over a permeable moving flat plate*. Phys. Scr. **86**(2012), 6, 045003.

[28] Rana P., Shukla N., Bég O.A., Bhardwaj A.: *Lie group analysis of nanofluid slip flow with Stefan blowing effect via modified Buongiorno's model: entropy generation analysis*. Differ. Equ. Dyn. Syst. **29**(2021), 193–210.

[29] Song Y.Q., Khan S.A., Imran M., Waqas H., Khan S.U., Khan M.I., Chu Y.M.: *Applications of modified Darcy law and nonlinear thermal radiation in bioconvection flow of micropolar nanofluid over an off centered rotating disk*. Alexandr. Eng. J. **60**(2021), 5, 4607–4618.

[30] Alsabery A. I., Tayebi T., Kadhim H. T., Ghalambaz M., Hashim I., Chamkha A. J.: *Impact of two-phase hybrid nanofluid approach on mixed convection inside wavy lid-driven cavity having localized solid block*. J. Adv. Res. **30**(2021), 63–74.

[31] Turkyilmazoglu M., Pop I.: *Heat and mass transfer of unsteady natural convection flow of some nanofluids past a vertical infinite flat plate with radiation effect*. Int. J. Heat Mass Tran. **59**(2013), 167–171.

[32] Hayat T., Muhammad T., Shehzad S. A., Alsaedi A.: *Three-dimensional boundary layer flow of Maxwell nanofluid: mathematical model*. Appl. Math. Mech. **36**(2015), 6, 747–762.

[33] Sheikholeslami M., Shehzad S. A.: *Simulation of water based nanofluid convective flow inside a porous enclosure via non-equilibrium model*. Int. J. Heat Mass Transf. **120**(2018), 1200–1212.

[34] Sarkar A., Das K., Kundu P.K.: *On the onset of bioconvection in nanofluid containing gyrotactic microorganisms and nanoparticles saturating a non-Darcian porous medium*. J. Mol. Liq. **223**(2016), 725–733.

www.czasopisma.pan.pl PAN POLSKA AKADEMIA NAUK www.journals.pan.pl

[35] Vajravelu K., Nayfeh J.: *Hydromagnetic convection at a cone and a wedge*. Int. Commun. Heat Mass Transf. **19**(1992), 701–710.

[36] Chamkha A.J.: *Non-Darcy hydromagnetic free convection from a cone and a wedge in porous media*. Int. Commun. Heat Mass Transf. **23**(1996), 875–887.

[37] Rao BM., Gopal D., Kishan N., Ahmed S., Prasad P.D.: *Heat and mass transfer mechanism on three-dimensional flow of inclined magneto Carreau nanofluid with chemical reaction*. Arch. Thermodyn. **41**(2020), 6, 223–38.

[38] Sathyanarayana M., Ramakrishna Goud T.: *Characteristics of MHD nanofluid flow towards a vertical cone under convective cross-diffusion effects through numerical solutions*. Heat Transfer. **52**(2022), 2, 1734–1753.

[39] Archana M., Gireesha B.J., Rashidi M.M., Prasannakumara B.C., Gorla R.S.: *Bidirectionally stretched flow of Jeffrey liquid with nanoparticles, Rosseland radiation and variable thermal conductivity*. Arch. Thermodyn. **39**(2018), 4, 33–57.